Substitution of Thoria Additions by Lanthanum-Oxide Doping in Electrodes for Atmospheric Plasma Spraying

M. Heißl*, C. Mitterer*, T. Granzer**, J. Schröder**, M. Kathrein***

* Department of Physical Metallurgy and Materials Testing, Montanuniversität Leoben, 8700 Leoben, Austria

** PLANSEE Composite Materials GmbH, 86983 Lechbruck, Germany

*** PLANSEE SE, 6600 Reutte, Austria

Abstract

Thoria (ThO_2) additions are used in tungsten-based electrodes for plasma spraying due to the excellent electron emissivity, improved arcing behavior, higher strength and better machinability. Because of their radioactive potential, which makes handling, use, recycling and disposal more difficult, research is done on alternative additives that provide at least the same advantages as thoriated tungsten but without environmental hazards. One of the most competitive alternatives to replace thoria is lanthania (La_2O_3). Within this work, tungsten cathodes with 2 wt.% thoria and 1 wt.% lanthania, respectively, were compared. Tests in terms of arc ignition, plasma stability and arc erosion, both in cyclic and continuous plasma spraying experiments were carried out. In addition, structure and mechanical properties of Al_2O_3 coatings sprayed on Mo substrates were evaluated. Lanthania is characterized by a similar plasma ignition and operation behaviour as well as a comparable coating quality with respect to thoria additions. Further, lanthania additions caused a reduced degradation of the cathode material, which is attributed to the lower cathode temperature, giving rise to an expected longer lifetime.

Keywords

Atmospheric plasma spraying, tungsten electrodes, thorium dioxide, lanthanum oxide

Introduction

In all industrial areas, increasingly higher demands are placed on materials in order to increase capacity of production and efficiency. To prevent premature failure or loss of function of a component, surface modifications or coating technologies are often applied. A frequently used coating method is thermal spraying, which contains numerous technologically different techniques, including flame spraying, arc spraying and plasma spraying [1]. Basically, a plasma spray process includes a spray material to be applied to a surface, which is transported to a so-called plasma torch. There it is heated and accelerated

onto the surface to be coated [2]. A major advantage is the wide range of materials that can be processed [3]. The quality of the coatings is largely dependent on the energetic conditions of the spraying device, in particular the contribution of the thermal and kinetic energy in the injected material [4]. Especially for the production of high-melting oxide ceramics, atmospheric plasma spraying is very useful since it provides sufficient thermal energy to melt these materials [5]. For the generation of the plasma, an electric arc is ignited between a pin-shaped cathode and a nozzle-shaped anode. These electrodes are worn out by repeated arc striking and arc erosion at high temperatures. The standard material for such an electrode is thoriated tungsten since it has excellent ignition properties. As this material is radioactive, research is done to replace it by more environmentally friendly materials. In tungsten inert gas welding, alternatives have already been found and approved [6]. The aim of this work is thus to demonstrate on the basis of a comparative study that tungsten with added lanthanum oxide could be used successfully instead of thoriated tungsten.

Experimental

Plasma spraying experiments have been conducted using a Sulzer Metco F4-HB plasma spraying torch mounted onto a robotic spraying system. This plasma torch is equipped with a water-cooling system to transfer heat from the electrodes and to prolong their lifetime. The water connection is also used to provide electrical power. The arc is ignited using a pen-shaped tungsten-tipped cathode and a tungsten-lined anode, which is set up as a nozzle [7]. Two tungsten-based electrode materials have been compared, i.e. tungsten with 2 wt.% ThO_2 and with 1 wt.% La_2O_3, respectively (denoted as WT20 and WL10 in the following). A mixture of argon and hydrogen has been used as plasma gas. A Sulzer Metco 9MP powder feeder was used to provide Al_2O_3 powder with a median particle size of 25.9 µm provided by Sulzer Metco. Coatings were sprayed on grit-blasted molybdenum plates (ø 58 mm × 3 mm). The spraying parameters are listed in Table I.

Table I: Parameters of the spraying process

Parameter	Value
Electrical current	630 A
Electrical power	~ 45 kW
Initial arc voltage	~ 71 V
Distance from substrate to spraying gun	180 mm
Intended total layer thickness	150 µm
Number of layers	2
Powder feed rate	35 g/min
Powder injection angle	90°
Powder carrier gas	Ar (8.5 l/min)
Process gas	Ar (40 l/min), H_2 (12 l/min)

To simulate repeated start and shutdown processes, 50 cycles with 5 minutes duration were carried out. The long term stability was studied for spraying over 20 hours, with short inspection interruptions after 5

minutes, 1, 5 and 10 hours. Emphasis was layed on evalutation of the process parameters electrical current and arc voltage as well as flow rate and temperature of the cooling water. To illuminate the effect of electrode erosion on coating properties, coatings were sprayed after every fifth cycle in the cyclical mode and before the inspection breaks in the continuous mode.

During the inspection breaks, the electrodes were examined using an endoscope of type TLX-2 Xenon by Richard Wolf. In addition a dial indicator of type MarCator 1096R by Mahr was used to estimate the change in length of the cathode by measuring the distance from the nozzle exit to the tip of the cathode. After both, cyclic and continuous tests, the worn cathodes were examined by scanning electron microscopy (SEM Carl Zeiss Ultra 55 plus). Metallographic cross-sections were investigated by optical microscopy using a Reichert-Jung Polyvar MET microscope. Coating quality was evaluated by measuring thickness and porosity on metallographic cross-section using optical microscopy and image analysis by the Olympus analySIS software.

Results and Discussion

Recording of the various process parameters in plasma spraying allows evaluation of changes of the electrode materials with time. Fig. 1(a) shows that in the cyclic mode the WT20 electrode starts at a slightly higher arc voltage of 72.2 V, compared to an initial value of 71.9 V for the WL10 electrode. This small difference is rather attributed to the accuracy of centering the cathode during installation than on differences of the electrode materials. The decline of the voltage starts after about 20 cycles in the case of WT20. In the experiment with WL10, the voltage drop was observed right from the beginning. The polynomial fit indicates that the curves approach each other at the end of the cyclic experiment, because the declining rate of WT20 increases. After 50 cycles the arc voltage is still far-off the limit of 60 V, which is used as an indicator for electrode replacement. In continuous mode (Fig. 1(b)), both electrodes start at a very similar arc voltage of approximately 72 V. Until 10 hours of uptime they are very much alike, dropping to a voltage of a about 70 V. But from that point on, they show a different behaviour. In the case of WT20, the voltage drops further and reaches 68 V after 20 hours of arc burning, while WL10 keeps a constant, higher voltage value. Hence, in terms of long-time operation the WL10-electrode shows a superior performance.

Since the electrical power P_{el} is the product of arc voltage and arc current, where the latter is held constant, it follows the trend shown in Fig. 1. By subtracting the dissipated power P_{diss}, which is transferred to the cooling water, the net plasma power can be estimated. P_{diss} can be calculated by a calorimetric approach, since the temperature difference $\Delta T_{i/o}$ between water inlet and outlet and the flow rate of the cooling water $\dot{m}_{H_2O}$ are known. With c_{H_2O} as the heat capacity of water (4184 J/K kg), one obtains:

$$\mathrm{P_{diss}} = \dot{\mathrm{m}}_{\mathrm{H_2O}} \cdot \mathrm{c}_{\mathrm{H_2O}} \cdot \Delta \mathrm{T}_{\mathrm{i/o}} \qquad (1)$$

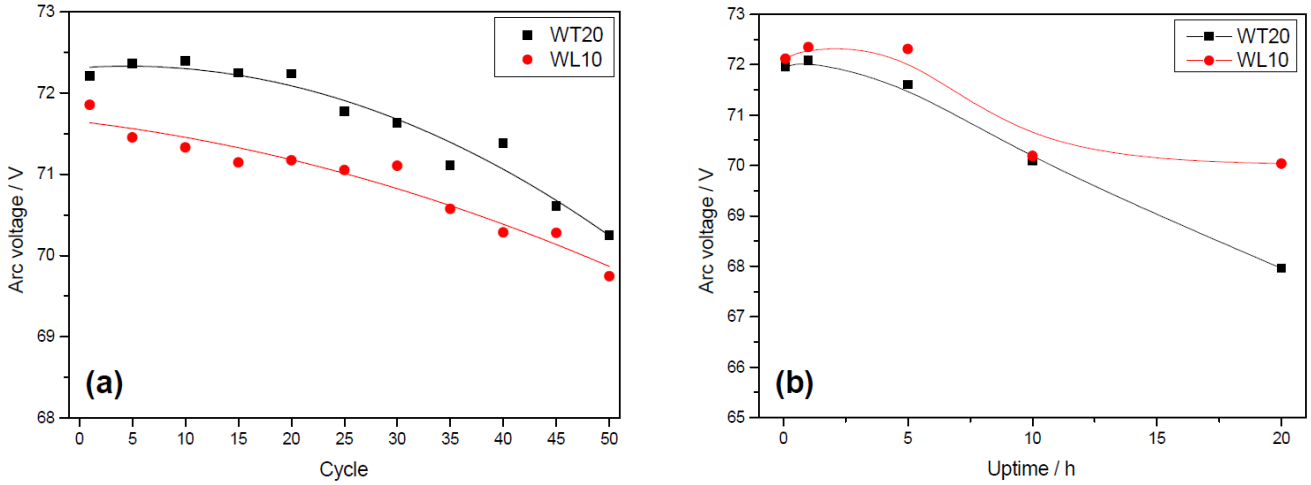

Figure 1: Arc voltage as a function of (a) number of cycles and (b) uptime for the electrode materials WT20 and WL10.

Then, the net plasma power P_{plasma} can be calculated:

$$\mathrm{P_{plasma} = P_{el} - P_{diss}} \qquad (2)$$

Fig. 2(a) shows that the thus derived dissipated power is slightly higher for WT20 than for WL10. As a consequence, the plasma power is nearly the same for both electrodes, although WL10 has a lower electrical power because of the lower arc voltage (see Fig. 1). Fig. 2(b) indicates that the cooling water is quickly heated up during the first cycles and reaches a constant level between 15 and 25 cycles. In the case of WT20, both heating rate as well as plateau are significantly higher than for WL10. Since the water flow rate is the same, this is an indication that the WT20 electrode is operating at a higher temperature. This is in accordance with its higher work function for electron emission (3.03 eV compared to 2.71 eV [8]), because a higher temperature is needed to reach the same emission current density.

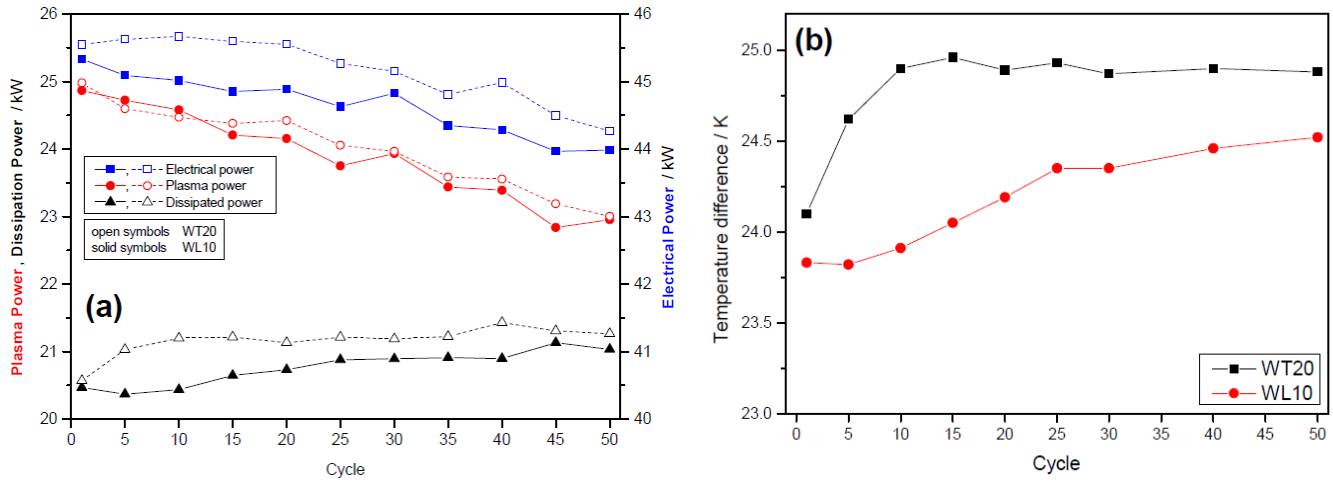

Figure 2: (a) Electrical, plasma and dissipated power and (b) temperature difference of cooling water at inlet and outlet as a function of number of cycles for the electrode materials WT20 and WL10.

Using the same approach for the continuous mode, WL10 is also superior to WT20 (see Fig. 3). The dissipated power is quite constant for both electrode materials during the continuous experiment, but always slightly higher in the case of WT20. Consequently, also the remaining plasma power is higher for WL10 than for WT20 (Fig. 3(a)). For the cooling water, very similar results are obtained as in the cyclic experiment. Independent of the electrode material, the temperature difference at outlet and inlet increases during the first five hours of arc burning time and then remains constant (Fig 3(b)). For all data points recorded, higher water temperatures have been obtained for WT20 compared to WL10, indicating higher WT20 electrode temperatures.

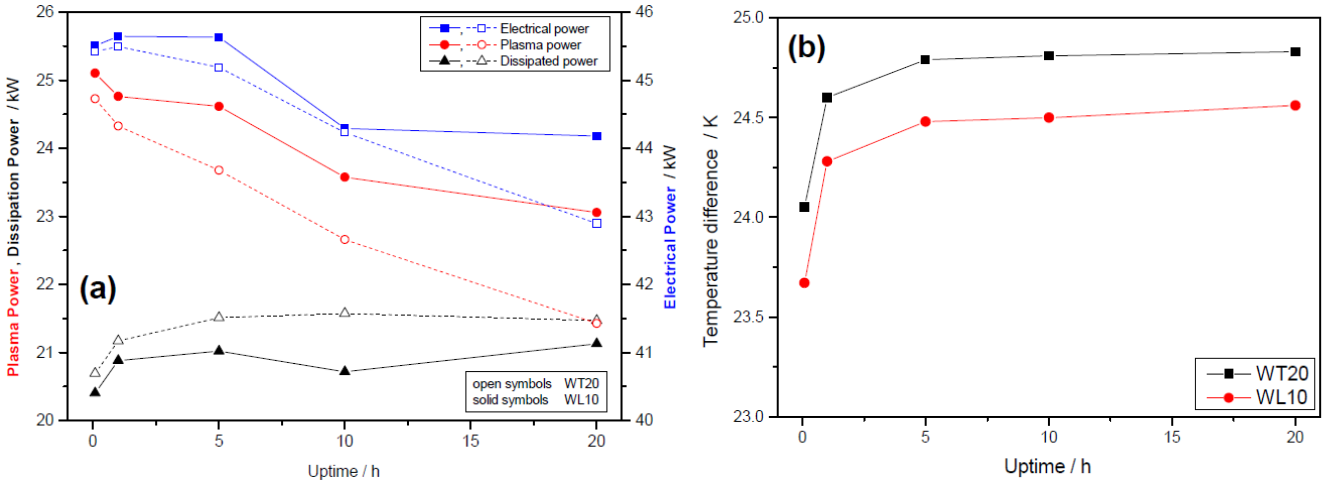

Figure 3: (a) Electrical, plasma and dissipated power and (b) temperature difference of cooling water at inlet and outlet as a function of uptime for the electrode materials WT20 and WL10.

The results of the measurements of change in length of the electrodes during the continuous experiment confirm the assumption, that WL10 is superior in terms of wearout during arc burning (see Fig. 4). While the WL10 electrode looses just 0.3 mm in length after 20 hours, the WT20 electrode shortens by more than 1.5 mm. The increasing difference in length with uptime corresponds to the increasing gap in the arc voltage for both materials (see Fig. 1(b)).

Figs. 5 and 6 illustrate the changes of the cathode tips after the cyclic experiments. After just ten ignitions of the WT20 electrode, small peaks are formed along the circumference, i.e. a so-called “corona structure” develops (see Fig. 5(a) for 20 cycles). The center is roughened up uniformly. The peaks grow with increasing number of cycles. At the end, the cathode tip shows eleven of those peaks, which are characterized by a reflecting surface, indicating that these domains may have melted during arcing. The peaks have a diameter of approximately 400 to 500 µm (see Fig. 5(b)). The phenomena leading to formation of the corona structure may result from local inhomogeneities close to the surface of the electrode material, developing gradually during arcing.

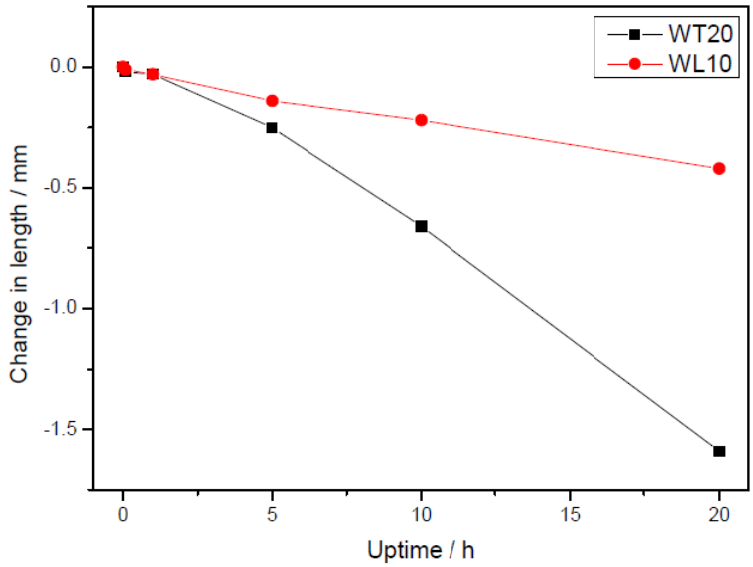

Figure 4: Change in cathode tip length as a function of uptime for the electrode materials WT20 and WL10 .

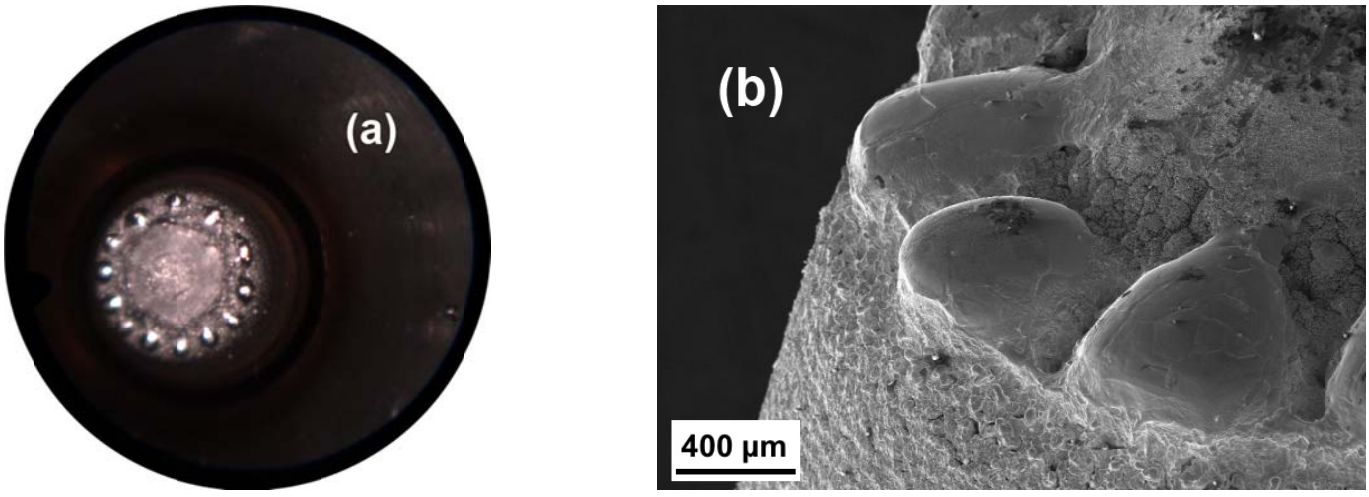

Figure 5: WT20 cathode after (a) 20 ignitions (endoscope) and (b) after 50 ignitions (SEM).

In contrast, the WL10 cathode shows a completely different behaviour (see Fig. 6). With increasing number of cycles, the cathode tip is flattened but remains smooth. A circular area with a mirror-like edge zone is formed. It is reasonable to assume that the arc attachment spot moves along the circumference of this area, because it is forced to this movement by the process gas. Therefore, the temperature at the edge may reach the melting point of the material.

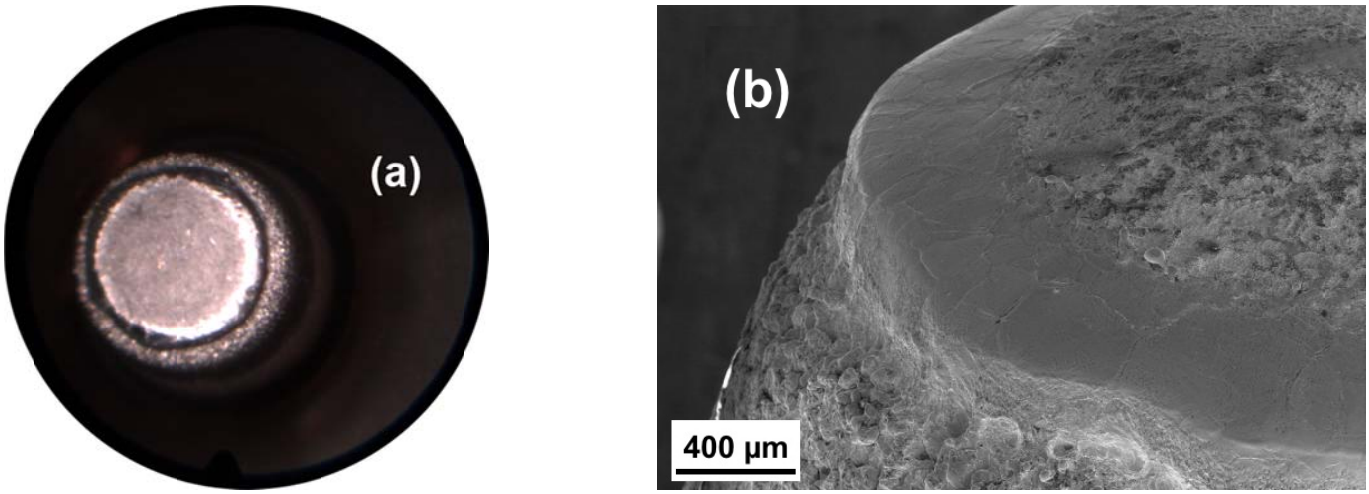

Figure 6: WL10 cathode after (a) 20 ignitions (endoscope) and (b) after 40 ignitions (SEM).

Studying the microstructure of the cathode tips after use reveals information about oxide distribution and grain size. Hardly any differences can be found between electrodes under cyclic and continuous load, but the two materials differ strongly from each other. The properties of each material are illustrated by a comparison of metallographic cross-sections of continuously loaded electrodes (Fig. 7). In the region far from the tip, both materials have a similar structure, characterized by fine grain size and a homogeneous distribution of oxides (left part of Figs. 7(a) and (b)). The grains have a longitudinal shape and are oriented along the cathode axis, which is a consequence of manufacturing. Closer to the tip, a coarsening of the structure is observed. The grain size in longitudinal direction is in the millimetre range, while in transverse direction it varies between 50 and 200 µm in the case of WT20 and is even more for WL10. The area around the tip is the most critical region, because this is where the arc is attached. This is also the area, where significant differences between the two materials occur. Fig. 7(a) evidences that at the tip of the WT20 cathode, the oxide dispersions are lacking in a region of approximately 1 mm from the tip. Therefore, the tip of the WT20 cathode works essentially as pure tungsten without significant emission enhancement caused by oxides. It is also noteworthy, that the transition to the region where oxides are present is very sharp. Since finely distributed oxide particles prevent grain growth during recrystallization by pinning grain boundaries, a finer microstructure is present in the area, where oxides exist, while in the oxide-free region coarsening sets in [9]. In contrast to WT20, oxides are still observed at the tip of the WL10 cathode (Fig. 7(b)). At the surface, only a small zone with a width of about 100 µm is free of oxides. This zone consists of a few big grains, since grain growth is hardly inhibited.

The effect of the increasing wear of the electrodes on the Al_2O_3 coating quality was investigated by a comparison of the first and last coatings for each spraying process with an intended coating thickness set to 150 µm. SEM investigations of metallographic cross-sections did not reveal significant differences in coating morphology. By comparing the first and the last sprayed coating, a decrease of coating thickness by 3 – 5 % was obtained for both electrode materials and operation modes. However, a comparison of the porosity of the coatings P_c reveals differences for the electrode materials. Although the coatings produced with WL10 electrodes have a slightly higher initial porosity (7 – 8 % compared to 6 – 7 % for WT20), the increase is smaller compared to the coatings using WT20 (10 – 11 % for WL10 compared to 11 – 12 % for WT20). This indicates a slightly more pronounced quality loss for WT20 with increasing wear of the electrodes.

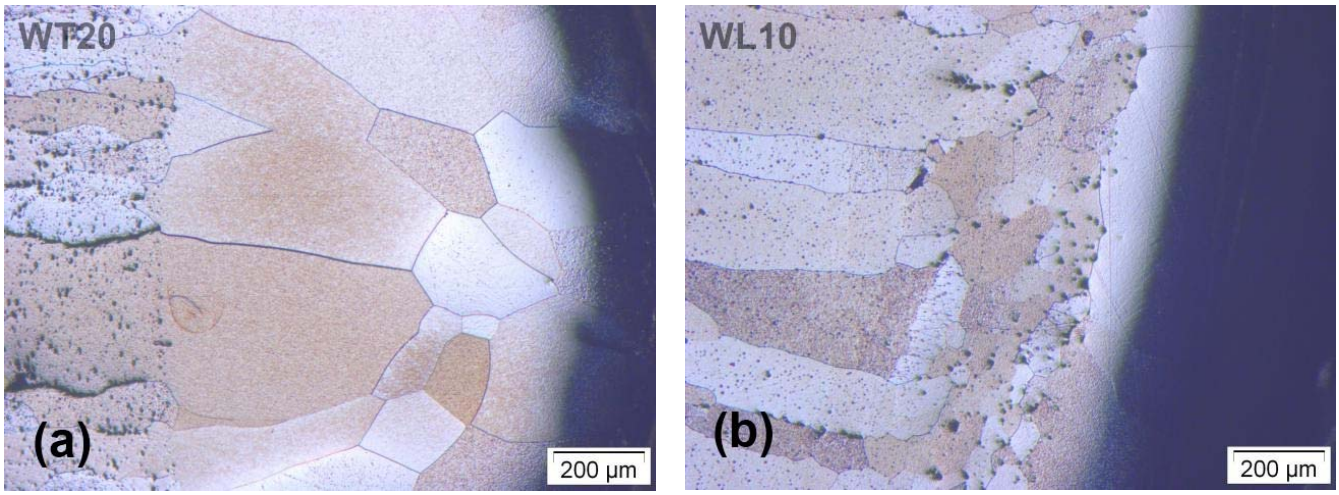

Figure 7: Optical micrographs of the structure at the cathode tip region. (a) WT20, (b) WL10.

The quality of the spraying process can be estimated by its deposition efficiency DE, which is the relationship of the mass of the actually deposited material m_{dep} to the mass of the totally used powder m_{tot} on the coated area A_c:

$$\mathrm{DE} = \frac{\mathrm{m_{dep}}}{\mathrm{m_{tot}}} \tag{3}$$

The mass of the deposited material m_{dep} for a given coating thickness s_c can be estimated by:

$$\mathrm{m_{dep}} = s_c \cdot \mathrm{A_c} \cdot \rho_c \cdot (1 - \mathrm{P_c}) \tag{4}$$

There, the density of the coating material ρ_c is 3.97 g/cm^3 for Al_2O_3 [10]. To calculate the mass of the used powder m_{tot}, the powder feed rate $\dot{m}_p$ and the total spraying time Δt must be known. The powder feed rate was set to 35 g/min (see Table 1) and the time was set to 5 minutes. The total sprayed area A_{tot} was approximately 1,274 cm^3. By setting this area in relation to the coated area A_c, which was 26.4 cm^3, and multiplying with the totally used powder mass m_{tot}, one obtains the net mass of powder used on the coated area:

$$\mathrm{m_{tot}} = \dot{\mathrm{m}}_\mathrm{p} \cdot \Delta \mathrm{t} \cdot \frac{\mathrm{A_c}}{\mathrm{A_{tot}}} \tag{5}$$

Eq. (5) yields a total mass m_{tot} of approximately 3.6 g. With the mass of deposited material m_{dep} according to Eq. (4) and the total mass m_{tot}, the deposition efficiency DE was calculated (Eq. (3)). DE was about 39 – 40 % for the first spraying processes, independent of the electrode material and the process mode. However, for the last sprayed coating of both the cyclic and the continuous mode, a decrease of DE was observed, with values of 36.5 – 38 % for WL10 and 35.5 – 36.5 % for WT20. The more pronounced decrease of DE in the case of WT20 shows that the WL10 electrodes outmatch those made of WT20 in terms of long-term use with constant process and coating quality.

Conclusion

Tungsten cathodes with 2 wt.% thoria (WT20) and 1 wt.% lanthania (WL10), respectively, were compared to elucidate the potential of lanthania to replace thoriated tungsten electrodes for plasma spraying. Tests in terms of arc ignition, plasma stability and arc erosion, both in cyclic and continuous plasma spraying experiments, were carried out. In addition, the structure both of the cathode tips and Al_2O_3 coatings sprayed on Mo substrates were evaluated in metallographic cross-sections.

In cyclic as well as continuous atmospheric plasma spraying experiments, the dropping rate of the arc voltage is lower for WL10; thus a longer service life can be expected. This is also evident from the observation of the erosion rate. Because of their lower work function, WL10 electrodes emit electrons more easily than WT20. Thus, less electrical power is required, because a lower temperature level is sufficient to sustain the plasma generating arc. Still, the net plasma power is the same, because in the case of WT20 more power is dissipated. These differences also affect the structural changes of the electrodes during spraying, where at the tip of the WT20 cathode no oxides are observed and the grain structure is coarse. Presumably, the temperature at the tip is sufficiently high to evaporate the oxides and to recrystallize its structure. In contrast, oxides are still present at the tip region of the WL10 cathode, providing enhancement of electron emission. The lanthania additions cause a reduced degradation of the cathode material, which is attributed to the lower cathode temperature. The increasing wear of the electrodes affects the quality of the coating. As the wearout is less in the case of WL10 cathodes, the coating quality is kept at a higher level for a longer period of time. The results show that it is not necessary to use thoriated electrodes, because lanthanum electrodes have a high potential to replace them.

References

1. J.R. Davis, *Handbook of Thermal Spray Technology*, ASM International Thermal Spray Society, Materials Park, Ohio, (2004)
2. C. Herbst-Dederichs, *Grundlagen des thermischen Spritzens*, in *Handbuch des thermischen Spritzens*, E. Lugscheider Ed., DVS Verlag, Düsseldorf, pp. 6-30, (2002)
3. Z. Babiak and T. Wenz, *Grundlagen der thermischen Spritztechnik*, in *Moderne Beschichtungsverfahren*, F.-W. Bach, K. Möhwald, A. Laarmann and T. Went Eds., Wiley-VCH, Weinheim, pp. 131-150, (2005)
4. Linde Gas, *Linspray – the noble art of coating. Gases and Know-how for Thermal Spraying*, Linde Gases Divison, Pullach (2005)
5. L. Pawlowski, *The Science and Engineering of Thermal Spray Coatings*, John Wiley & Sons, Chichester, (2008)
6. A. Sadek, M. Ushio and F. Matsuda, *Metall. Mater. Trans. A* **21** [12], 3221-3237, (1990)
7. Sulzer Metco, *Product Data Sheet F4MB-XL Series*, Winterthur, (2011)
8. G. Leichtfried, *Powder Metallurgical Components for Light Sources*, Ph.D. thesis, Montanuniversität, Leoben, (2003)
9. G. Gottstein, *Physikalische Grundlagen der Materialkunde*, Springer, Berlin, (2007)

10. J.F. Shackelford and W. Alexander, *Materials Science and Engineering Handbook*, 3rd edition, CRC Press, Boca Raton, (2001)